Normalization of T2W-MRI Prostate Images using Rician a priori

G. Lemaître, M. Rastgoo, J. Massich, J. C. Villanova, P. M. Walker, J. Freixenet, A. Meyer-Baese, F. Mériaudeau, and R. Martí

LE2I - Université de Bourgogne Franche-Comté / ViCOROB - Universitat de Girona

Introduction

- Prostate Cancer (CaP) has been reported the **second** most frequently diagnosed cancer of men accounting for 13.6% [F+10].
- Computer-Aided Diagnosis systems have been proposed in order to assist the radiologists and generally consist of four stages: (i) **pre-processing**, (ii) *segmentation*, (iii) *registration*, and (iv) *classification* [L+15].
- **Normalization** is crucial to overcome the *inter-patient* intensity variations, enforce the *repeatability*, and achieve a *robust* classification.

State-of-the-art method

- Artan *et al.* [A+10] and Ozer *et al.* [O+10] used the **z**-*score* (see Eq. (1)) to normalize T2W-MRI.
- Lv *et al.* [L+09] and Viswanath *et al.* [V+12] used methods based on piecewise-linear normalization [Nea00].

Contributions

We proposed two alternative methods:

(i) a *model-based* approach using Rician *a priori*;

(ii) a *non-parametric based* approach based on the Square-Root Slope Function (SRSF) representation [SKJJ11].

Model-based normalization

Gaussian normalization / Rician normalization

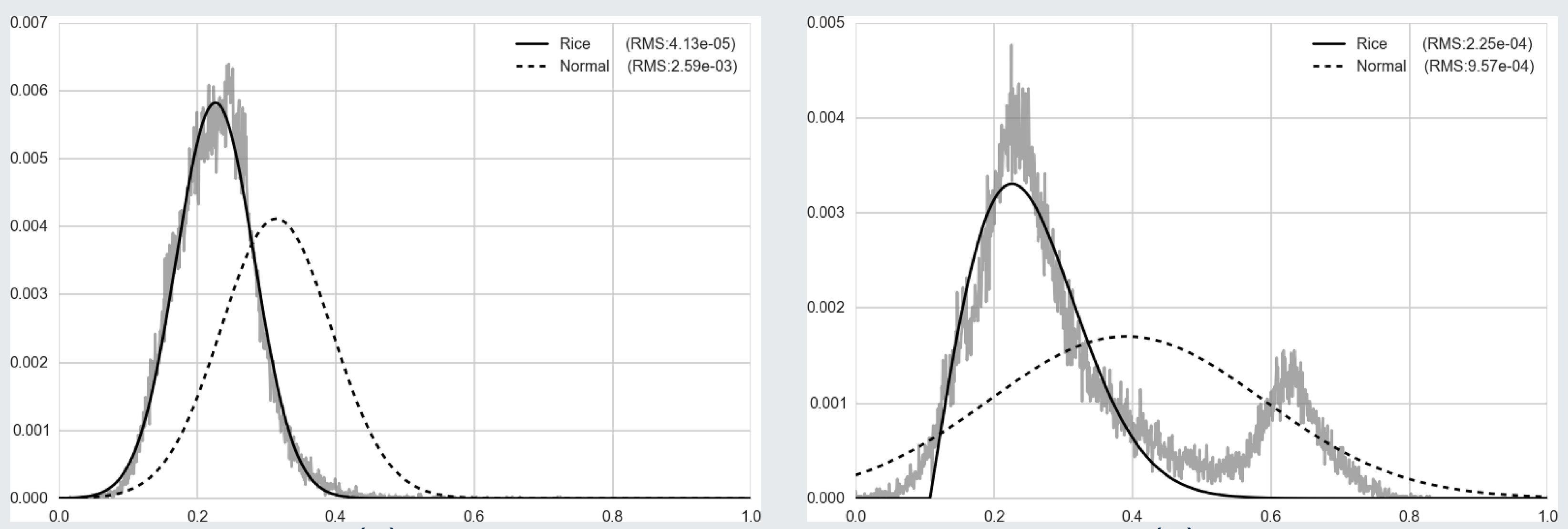

(a) (b)

Figure : Visual evaluation of the goodness of fitting using Rician and Gaussian distribution.

$$\mathbf{I_s(x)} = \frac{\mathbf{I_r(x)} - \mu_G}{\sigma_G} \ . \qquad (1)$$

$$\mathbf{I_s(x)} = \frac{\mathbf{I_r(x)} - \mu_R}{\sigma_R} \ , \qquad (2)$$

where,

$$\mu_R = \sigma \sqrt{\frac{\pi}{2}} \ \mathrm{L}_{1/2}\left(-\frac{\nu^2}{2\sigma^2}\right) , \qquad (3)$$

$$\sigma_R = 2\sigma^2 + \nu^2 - \frac{\pi\sigma^2}{2} \mathrm{L}_{1/2}^2 \left(\frac{-\nu^2}{2\sigma^2}\right) . \qquad (4)$$

- MRI data theoretically follows a Rayleigh distribution for a low SNR scenarios while it appears closer to a Gaussian distribution when the SNR increases [Bea89].
- The Rician model better fits the data than the Gaussian model in terms of RMS.

Non-parametric normalization

Piecewise-linear normalization / SRSF-based normalization

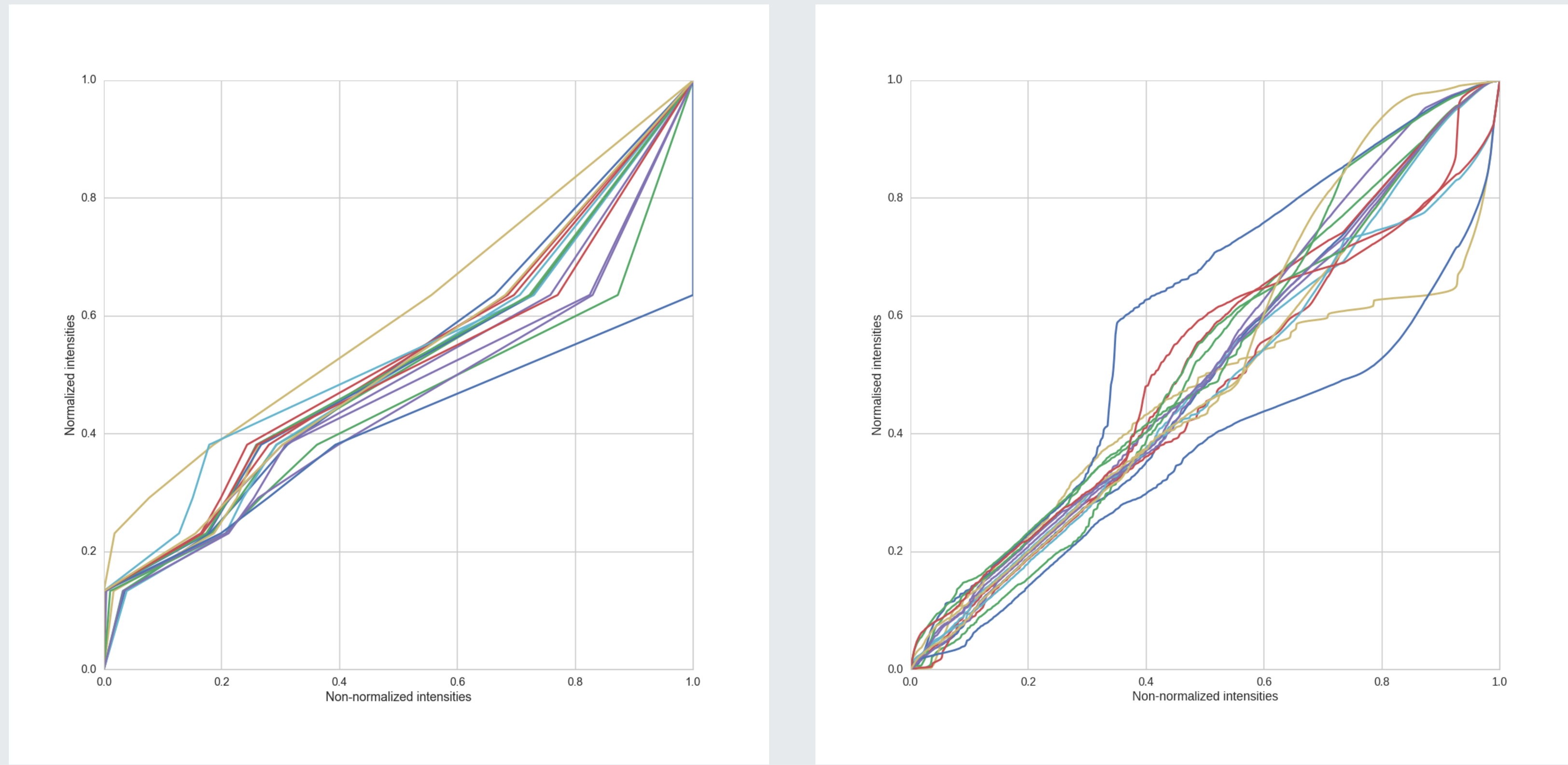

(a) (b)

Figure : Comparison of warping function obtained with (a) piecewise-linear normalization and (b) SRSF-based normalization.

- Minimize the distance between a set of standardized landmarks $\boldsymbol{\mu}_\mathbf{i}$ (i.e., atlas) and a set of non-normalized landmarks $\boldsymbol{\lambda}_\mathbf{i}$.

$$\underset{\mathbf{d}}{\arg\min}\ \mathbf{d}(\boldsymbol{\lambda}_\mathbf{i}, \boldsymbol{\mu}_\mathbf{i}) \ , \qquad (5)$$

- Minimize the distance between a mean PDF $\boldsymbol{\mu}_\mathbf{f}$ (i.e., the Karcher mean) and a given patient PDF $\mathbf{f_i}$.

$$\underset{\gamma \in \Gamma}{\arg\min}\ \mathbf{D_y}(\boldsymbol{\mu}_\mathbf{f}, \mathbf{f_i})^2 \ , \qquad (6)$$

- SRSF-based normalization lead to smoother transition than piecewise-linear normalization.
- SRSF-based normalization can get unstable due to the noise.

Quantitative results

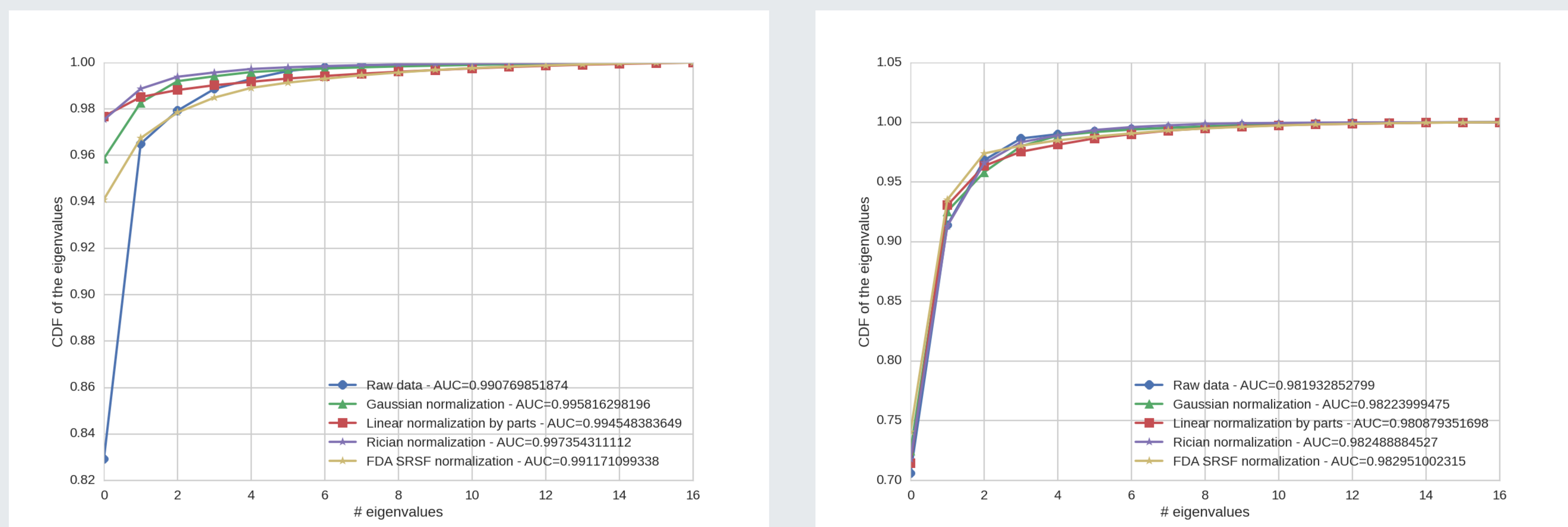

(a) (b)

Figure : Spectral evaluation using PCA decomposition: (a) evaluation considering the full prostate, (b) evaluation considering only the CaP.

- Rician normalization outperforms the other methods: Area Under this Curve of **0.9974** and **0.9824** considering the full prostate and CaP, respectively.

Qualitative results

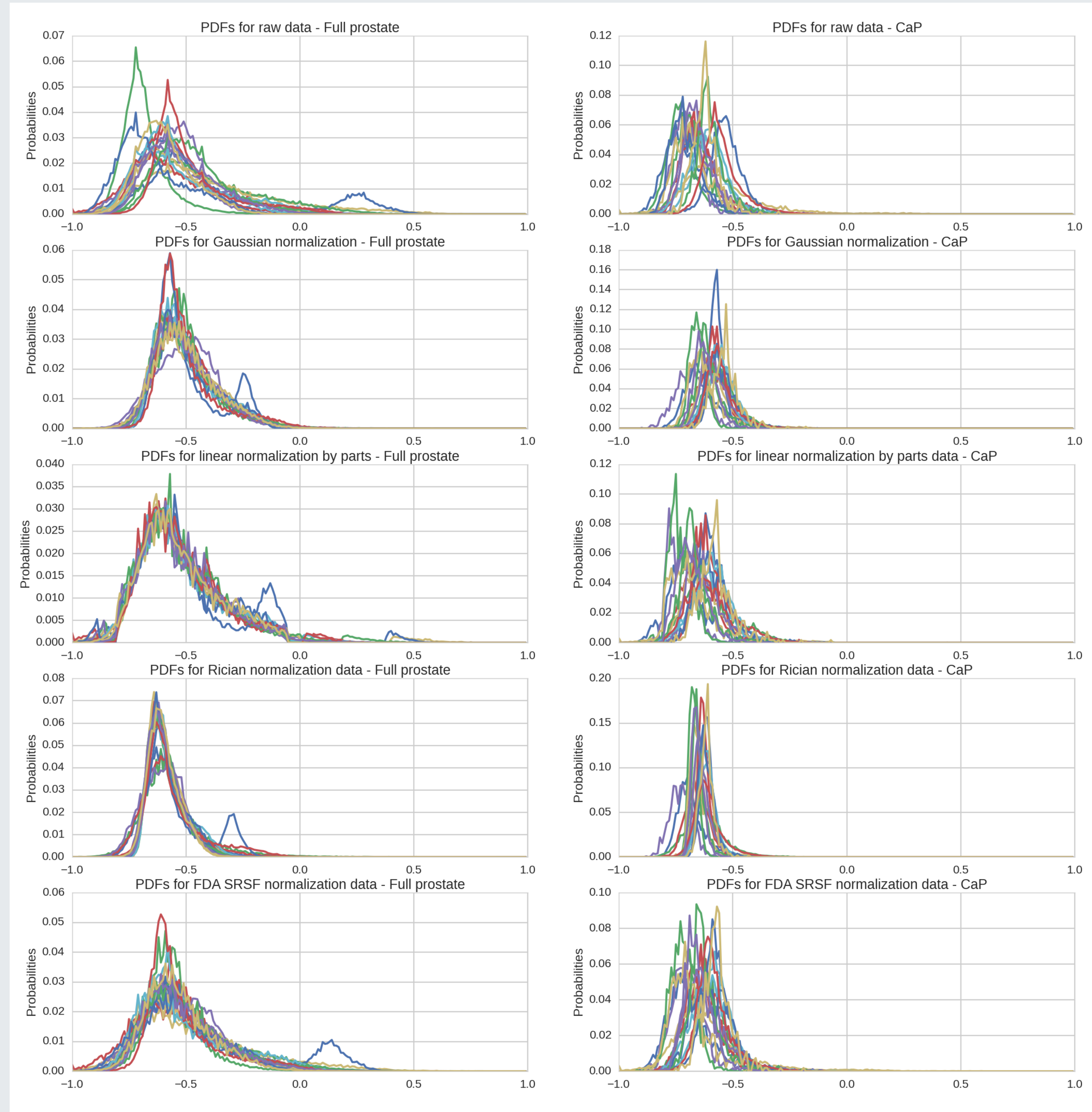

Figure : Qualitative evaluation by visual inspection of the alignment of the PDFs for the full prostate and the CaP.

- All the methods address the problem of the PDF alignment of the full prostate data.
- However, the Rician normalization outperforms the other methods when focusing solely on the CaP data.

Conclusion

Comparisons show that the Rician normalization outperforms the Gaussian, SRSF-based, and piecewise-linear normalization for T2W-MRI prostate images normalization.

References

[A+10] Yusuf Artan et al., *Prostate cancer localization with multispectral mri using cost-sensitive support vector machines and conditional random fields*, IEEE TIP **19** (2010), no. 9.

[Bea89] M. A. Bernstein and et al., *Improved detectability in low signal-to-noise ratio magnetic resonance images by means of a phasecorrected real reconstruction*, Medical Physics **16** (1989), no. 5.

[F+10] Jacques Ferlay et al., *Estimates of worldwide burden of cancer in 2008: Globocan 2008*, Int. journal of cancer **127** (2010), no. 12.

[L+09] Dongjiao Lv et al., *Computerized characterization of prostate cancer by fractal analysis in mr images*, JMRI **30** (2009), no. 1.

[L+15] Guillaume Lemaître et al., *Computer-aided detection and diagnosis for prostate cancer based on mono and multi-parametric mri: A review*, Comp. in Bio. Med. **60** (2015).

[Nea00] László G Nyúl and et al., *New variants of a method of mri scale standardization*, IEEE TMI **19** (2000), no. 2.

[O+10] Sedat Ozer et al., *Supervised and unsupervised methods for prostate cancer segmentation with multispectral mri*, Med. Phy. **37** (2010), no. 4.

[SKJJ11] A. Srivastava, E. Klassen, S.H. Joshi, and I.H. Jermyn, *Shape analysis of elastic curves in euclidean spaces*, Pattern Analysis and Machine Intelligence, IEEE Transactions on **33** (2011), no. 7.

[V+12] S. Viswanath et al., *Central gland and peripheral zone prostate tumors have significantly different quantitative imaging signatures on 3 tesla endorectal, in vivo t2-weighted mr imagery*, JMRI **36** (2012), no. 1.